Applied Physics A (2021) 127:606
https://doi.org/10.1007/s00339-021-04775-4

Applied Physics A
Materials Science & Processing

Binary nickel and silver oxides by thermal route: preparation and characterization

Eman Absi[1,2] · Muneer Aziz Saleh[3] · Naif Mohammed Al-Hada[4,5] · Khaidzir Hamzah[3] · Abdulsalam M. Alhawsawi[6,7] · Essam M. Banoqitah[8]

Received: 6 June 2021 / Accepted: 14 July 2021 / Published online: 19 July 2021

Abstract

Many studies have concentrated on exploring behaviors of nickel silver oxide nanoparticles using various routes of fabrication. Thermal treatment technique has never been utilized to fabricate nickel oxide silver oxide nanoparticles. In this research, binary $(NiO)_{0.4}$ $(Ag_2O)_{0.6}$ nanoparticles were synthesized using the thermal treatment method due to its attractive advantages such as low cost, eco-friendly, and purity of nanoparticles. The structural, morphological, and optical behaviors of these nanoparticles were investigated at different calcined temperatures. X-ray diffraction (XRD), transmission electron microscopy (TEM), energy-dispersive X-ray spectroscopy (EDX), X-ray photoelectron spectroscopy (XPS), ultraviolet–visible spectroscopy (UV–Vis), and photoluminescence (PL) were the techniques used to characterize the synthesized nanoparticles. XRD was conducted at different calcined temperatures. The crystallite size was increased from 25.4 nm to 37.0 nm as the calcined temperature increased from 500 °C to 800 °C. Also, TEM results verified that the mean particle size was enlarged as the calcined temperatures increased. Two band gaps were found for each temperature, which were decreased from (3.05, 2.45) to (2.70, 1.95) eV as the temperature varied from 500 to 800 °C, respectively. Broadbands were observed by PL spectra, and the intensity of two emission peaks was also increased at higher temperatures. The results approved the successful formation of binary $(NiO)_{0.4}$ $(Ag_2O)_{0.6}$ nanoparticles by a novel facile synthesis route. These nanoparticles are likely to have various applications, especially optical applications due to the formation of two band gaps.

Keywords $(NiO)_{0.4}$ $(Ag_2O)_{0.6}$ nanoparticles · Structural properties · Optical properties · Polyvinylpyrrolidone · Thermal treatment route

1 Introduction

Metal oxide nanoparticles (NPs) have resulted from the reaction between metal elements and oxygen. Nickel oxide (NiO) [1–9] and silver oxide (Ag_2O) NPs [10–18] were widely studied due to their valuable applications. Nickel oxide is a p-type semiconductor material [19–21], which has a wide band gap energy range of 3.6–4.0 eV [1, 20, 21]. Considerable interest in the properties of metal oxide NPs has been developed over the last few years [22, 23]. NiO NPs were

✉ Naif Mohammed Al-Hada
naifalhada@yahoo.com

1 Department of Physics, Faculty of Science, Universiti Teknologi Malaysia, Johor Bahru, Malaysia

2 Department of Coastal Environment, School of Basic and Marine Sciences, The University of Jordan-Aqaba Branch, Aqaba, Jordan

3 Nuclear Energy Programme, School of Chemical and Energy Engineering, Faculty of Engineering, Universiti Teknologi Malaysia, Johor Bahru, Malaysia

4 Shandong Key Laboratory of Biophysics, Institute of Biophysics, Dezhou University, Dezhou 253023, China

5 Department of Physics, Faculty of Applied Science, Thamar University, 87246 Dhamar, Yemen

6 Department of Nuclear Engineering, Faculty of Engineering, King Abdulaziz University, P.O. Box 80204, Jeddah 21589, Saudi Arabia

7 Center for Training & Radiation Prevention, King Abdulaziz University, P.O. Box 80204, Jeddah 21589, Saudi Arabia

8 Department of Nuclear Engineering, Faculty of Engineering, K. A. CARE Energy Research and Innovation Center, King Abdulaziz University, P.O. Box 80204, Jeddah 21589, Saudi Arabia

formed in different shapes: nanospheres [1–4, 7, 19, 24, 25], nanorods [5, 9], and thin films [8]. Different shapes were found in several studies for Ag_2O NPs such as cube, ellipsoid [10], and spherical shape [12–18, 26–28].

Because of its optical and electrical properties [2], the use of NiO NPs in various applications has been gradually increased. Also, NiO NPs are well known as antiferromagnetic materials [1]. Extensive applications of NiO NPs were reported in several studies such as electrochemical performance, sensors [3, 19, 29], biosensors [6], Li-ion batteries [4, 5], catalysts for hydrogen evolution reaction [3], fabrication of hybrid perovskite solar cells [7], energy storage and memristor technologies [8], optoelectronics [9], photocatalytic degradation [20], and antibacterial applications [2]. Conversely, Ag_2O is known as a p-type semiconductor with an energy band gap of 1.2 eV [30, 31]. Ag_2O NPs have been widely used as antimicrobial (antibacterial) agents [10–18, 32]. Other applications are also reported in different studies such as dye degradation and insecticidal activity [10], antifungal activity [11], photocatalytic agent for different uses [12, 14, 15, 31], antibacterial action against species of dental bacteria [13], anti-inflammatory, antioxidant, antidiabetic [18], cytotoxic, insecticidal, phytotoxic, antioxidant, anthelmintic agents [32], anticancer agent [16, 17], sensors [33], methanol sensing applications [28], pharmaceutical products, cosmetic, food industry, water treatment, gas sensing, electronics, construction materials, and paints industry [17], fuel cells, photovoltaic solar cells, optical switching, and data storage devices [26, 31, 34].

NiO and Ag_2O NPs have been fabricated by different synthesis routes in the current research studies. NiO NPs were synthesized by sol–gel [1, 7–9], a hydrothermal method [3, 5], thermal decomposition [4, 24], co-precipitation method [6], microwave combustion method [2], aqueous chemical growth procedure [29], and green synthesis procedures using Agathosma betulina plant extract [35], medicinal plant Prunus persica [19], Calotropis gigantea leave extract [36], and Ananas comosus leaf extract [20]. Conversely, Ag_2O NPs were synthesized by different synthesis routes: thermal decomposition [33], co-precipitation [17], simple chemical method [34], simple solution method [28], capping method [27], combustion method by Gomutra (cow urine) [15], and via green synthesis by using C. edulis extract [10], Daphne alpina [11], Lippia citriodora plant powder [12], Zephyranthes rosea flower extract [18], Ficus benghalensis prop root extract [13], Centella asiatica and tridax plant powder [14], Lactobacillus mindensis [26], and medicinal plant Cyathea nilgiriensis Holttum [16].

Also, many researchers fabricated nickel/silver [37–40] and silver nickel oxide NPs [41–47] by different synthesis routes. The mentioned methods are faced many limitations such as long procedure, use of many chemicals and reagents, relatively high cost, and some impurities that can be found in the final product. Therefore, the production of pure NPs using a method that is simple, inexpensive, and eco-friendly is highly required. Based on these advantages, the thermal treatment method was chosen for the synthesis of binary nickel oxide–silver oxide NPs for the first time to our knowledge. The effect of varying the temperature will be investigated on the prepared NPs. In this research, good optical properties will be achieved by producing NPs with two band gaps. The synthesized NPs can be used in applications and devices that require the absorption of a broad range of visible light.

2 Experimental method

2.1 Materials

The nickel (II) nitrate hexahydrate ($Ni(NO_3)_2.6H_2O$) and silver nitrate ($AgNO_3$) were taken as precursor materials for the synthesis of $(NiO)_{0.4}$ $(Ag_2O)_{0.6}$ NPs. Polyvinylpyrrolidone (PVP) was employed as a capping agent and a stabilizer to prevent aggregation. Reactions were carried out in deionized water as a solvent. $Ni(NO_3)_2.6H_2O$ (99%), $AgNO_3$ (99%), and PVP (99.99%, MW = 29,000 g mol^{-1}) were purchased from Acros Organics, Bendosen, and Sigma-Aldrich, respectively.

2.2 Methodology

In the current research, a simple thermal treatment method was employed to fabricate a novel binary material; namely, $(NiO)_{0.4}$ $(Ag_2O)_{0.6}$ NPs. PVP (0.5 g) was dissolved in deionized water (100 ml) at 80 °C. Then 0.004 mol (1.1632 g) of $Ni(NO_3)_2.6H_2O$ and 0.006 mol (1.0193 g) of $AgNO_3$ powders were dissolved in the solution of PVP and deionized water until all precursors were dissolved. The prepared solution was poured into Petri dishes and dried in an oven at 85 °C for 24 h. Each dried residue was crushed using mortar and pestle and then kept at room temperature for analysis. Finally, each residue was calcined in a furnace at 500, 600, 700, and 800 °C for 3 h at a heating rate of 3 °C min^{-1}. The prepared samples were taken for analysis by TGA, XRD, TEM, EDX, XPS, TEM, UV–Vis, and PL.

2.3 Characterization

The synthesized $(NiO)_{0.4}$ $(Ag_2O)_{0.6}$ NPs were analyzed using different characterization techniques (TGA, XRD, TEM, EDX, XPS, UV–Vis, and PL). A PerkinElmer thermogravimetric analyzer (TGA 4000) was used for thermal analysis. The analysis was operated by using N_2 as purging gas, at a heating rate of 10 °C min^{-1} within a temperature range from 30 ˚C to 900 °C. The structural properties

of the synthesized NPs were studied by X-ray diffraction (XRD), energy-dispersive X-ray spectroscopy (EDX), and X-ray photoelectron spectroscopy (XPS). XRD was investigated the crystal structure and the crystalline size of NPs. An XRD diffractometer (Rigaku-smart lab, Japan) with an X-ray source of Cu-Kα radiation of 0.154 nm, running at 40 kV and 30 mA, was employed for this purpose. All samples were scanned in the region between 3° and 90°. EDX was applied to identify the elemental composition of the prepared samples. It was carried out using an EDX spectrometer (Hitachi SU8020). XPS was also used to study the elemental composition, chemical and electronic states of elements found in the prepared NPs. The analysis was performed using Kratos Axis Ultra X-ray photoelectron spectrometer. Hitachi HT7700 transmission electron microscopy (TEM) was operated at an accelerating voltage of 200 kV to study the dimensions and morphology of the synthesized NPs. The optical properties of the prepared NPs were studied using UV–Vis spectrophotometer from PerkinElmer model (LAMBDA 1050). The optical reflection of the samples was recorded in a wavelength range between 200 and 850 nm, and its resolution reaches 0.05 nm. Also, the optical features were studied from photoluminescence (PL) measurements. The analysis was carried out using the PTI QuantaMaster™ 60 fluorescence spectrophotometer that equipped with xenon illuminator (75 Watts), xenon flash lamp, LEDs, and laser diodes.

3 Results and discussions

3.1 Mechanism of formation of binary metal oxide nanoparticles

The mechanism occurred for preparing binary $(NiO)_{0.4}$ $(Ag_2O)_{0.6}$ NPs is shown in Fig. 1. An interaction happened between ions (Ni^{2+} and Ag^{+}) and PVP in the solution. The powerful ionic bonds held all constituents together including the amide groups of the polymer chains and the metallic ions of the oxides. The metal precursors were dissolved with the existence of amide groups (in pyrrolidone rings) and methylene groups (in the polymer). Polymers are assumed to have an important role as a capping agent to the metallic ions when they were adsorbed to the surface. Initially, these short chains of the polymer were constructed due to the breakage has happened inside the stabilizer (PVP). In fact, homogeneous dispersion of metallic ions was certainly occurred throughout the polymer due to its short chain. While drying, water was removed, and hence, the mobility of metallic ions was frozen. Due to the oxidization of Ni^{2+} and Ag^{+} ions during heat treatment, $(NiO)_{0.4}$ $(Ag_2O)_{0.6}$ NPs had produced. The reaction that occurred between NiO and Ag_2O under heat treatment initiated the formation of the binary phases. Organic matter was eliminated, and NPs started merging as the temperature increased which caused the particle size with minimum surface energy to enlarge. The final role for

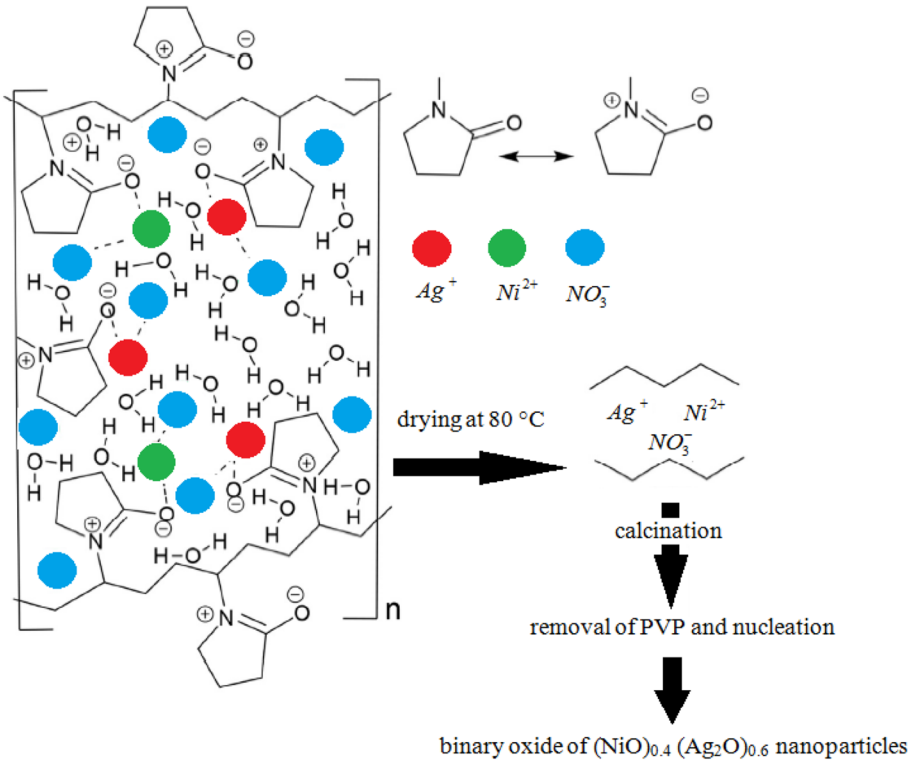

Fig. 1 Mechanism of reaction between precursors and PVP to produce binary $(NiO)_{0.4}$ $(Ag_2O)_{0.6}$ NPs

PVP in this study was the nucleation of $(NiO)_{0.4}$ $(Ag_2O)_{0.6}$ NPs during calcination. However, the use of PVP with a high molecular weight value (> 10,000 g mol^{-1}) has an advantage of minimizing the aggregation of smaller NPs due to the existence of polyvinyl groups, which have produced repulsive forces [48].

3.2 Thermal analysis

Thermal analysis of nickel nitrate, silver nitrate, and PVP was conducted by thermogravimetric (TGA) and differential thermal (DTG) analyses to identify the calcination optimal initial temperature. Figure 2 shows TG–DTA curves for the synthesized NPs, containing PVP (MW = 29,000 g mol^{-1}) and bimetallic nitrate before calcination. After calcination, four stages for loss of weight were appeared. The first loss was happened for trapping moisture from the sample, which observed above 200 °C. Two other small peaks resulted from the breakdown of organic compounds that appeared at 300 °C and below 400 °C. Finally, the majority of PVP had been broken down, so the highest weight loss was recorded at 424 °C. It was noticed that the variation in weight loss against temperature became insignificant at 464 °C, which indicates that the remainder of the PVP was decomposed completely into carbonaceous products. No additional weight loss was found above 464 °C. The removal of carbonaceous matter had happened within the range of 424–464 °C. The color was changed from green to dark gray, indicating the formation of high-purity NPs.

3.3 Structural characterizations

XRD diffraction patterns for $(NiO)_{0.4}$ $(Ag_2O)_{0.6}$ NPs before and after calcination are shown in Fig. 3. No diffraction peaks were appeared for NiO and Ag_2O at room temperature, which indicates that the sample is amorphous. After calcination, the crystals were formed so many diffraction peaks were appeared for both NiO and Ag_2O which are labeled by (*) and (#) symbols, respectively. The diffraction peaks of NiO were appeared at 2θ of 37.2°, 43.2°, 62.8°, 75.3°, and 79.2° which were indexed to (111), (200), (220), (311), and (222) plane indices, respectively. Conversely, the diffraction peaks of Ag_2O were found at 2θ of 38.1°, 44.2°, 64.4°, 77.3°, 81.5°, and 97.8° which were related to (111), (200), (220), (311), (222), and (400) plane indices, respectively. These results revealed that the synthesized nanoparticles by thermal treatment method is pure since no other peaks of impurities were appeared. It is also observed that the crystallinity of the sample was enhanced as the temperature increased from 500 to 800 °C. The intensity of the peaks increased and hence the crystallite size was grown from 25.4 to 37.0 nm (Table 1). In fact, the crystallite size was evaluated through the Debye–Scherrer's equation:

$$D = \frac{0.94\lambda}{\beta \cos\theta} \tag{1}$$

where D is the crystallite size (Å), λ is the wavelength of X-ray source (nm), β is the intensity full width half maximum (FWHM) at (111) in this research, and θ is the diffraction angle [49, 50]. Cubic phase were found for NiO NPs which correlated with (DB card number 00-047-1049). Also, Ag_2O NPs contain cubic phase which are correlated with (DB card number 01-071-4613). So, $(NiO)_{0.4}$ $(Ag_2O)_{0.6}$ NPs were formed in a combination of these two cubic phases.

EDX analysis was done to confirm the formation of $(NiO)_{0.4}$ $(Ag_2O)_{0.6}$ NPs and also to determine its elemental

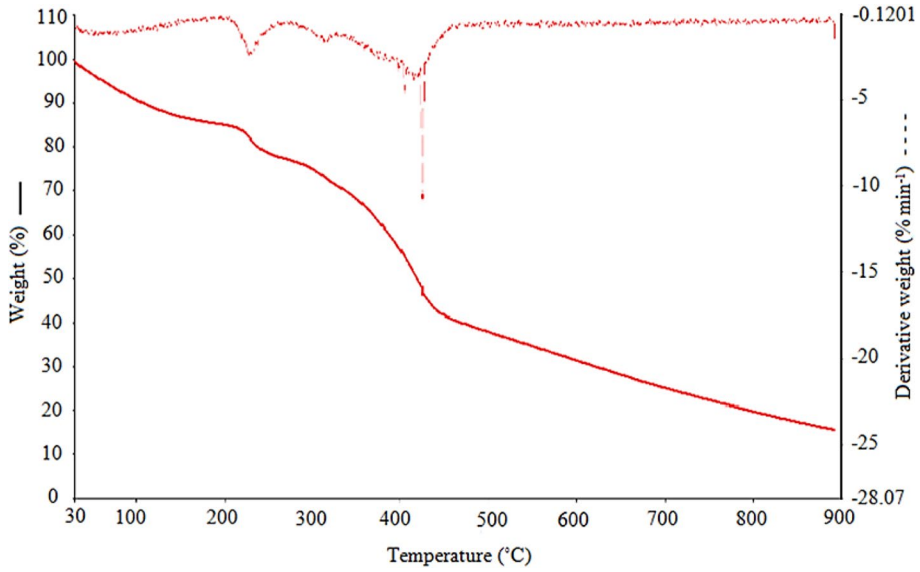

Fig. 2 TGA and DTG derivative curves for bimetallic nitrate and PVP at a heating rate of 10 °C/min

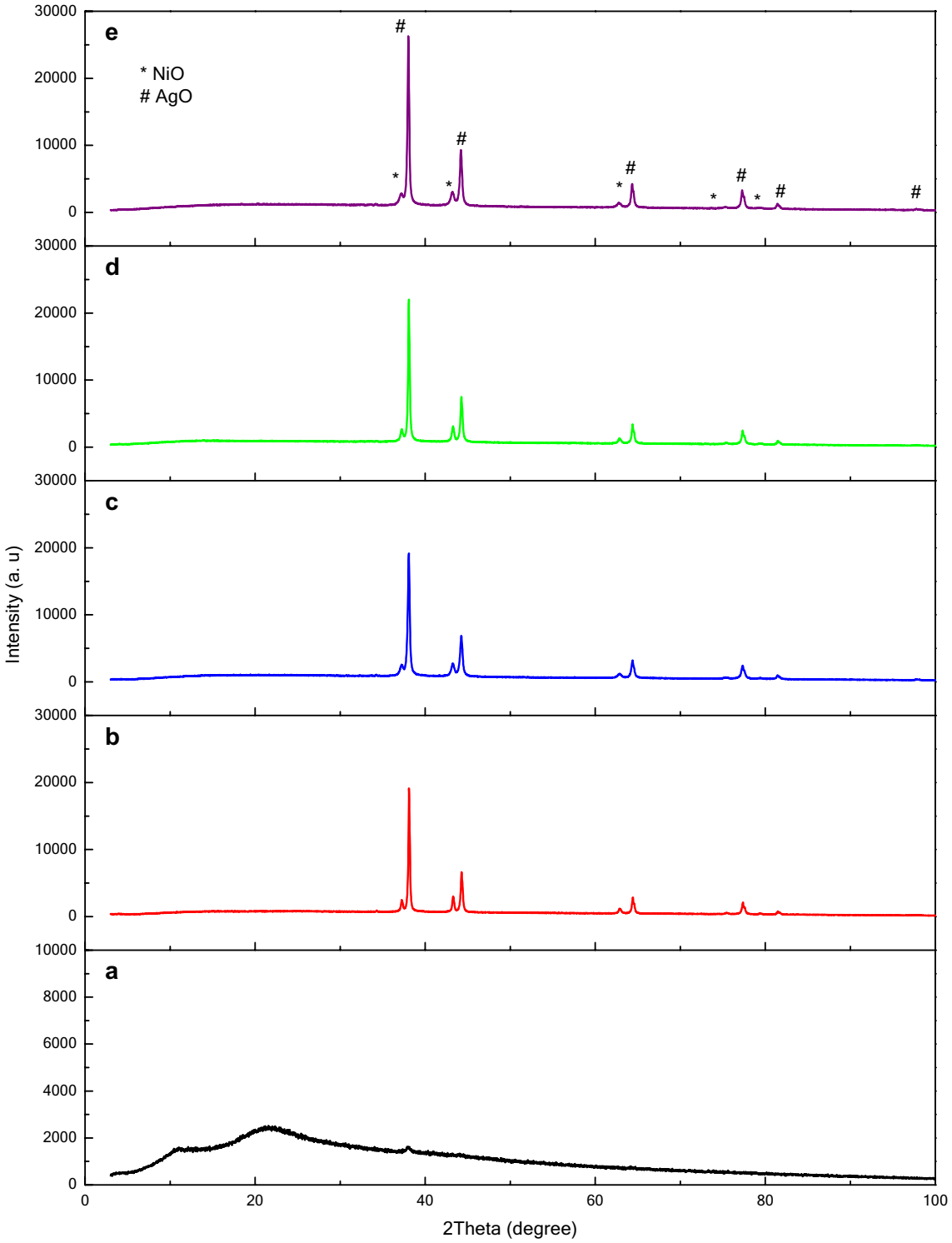

Fig. 3 XRD patterns of $(NiO)_{0.4}$ $(Ag_2O)_{0.6}$ NPs synthesized at **a** room temperature, **b** 500, **c** 600, **d** 700, and **e** 800 °C

composition that were calcined at 700 °C. The spectra proved the existence of Ni, Ag, and O via the equivalent peaks appeared in Fig. 4. The reason for the appearance of small carbon peaks might be due to the EDX holder during test the sample. However, minimal loss of elements was verified which reflects the degree of efficiency of this method [48].

Table 1 XRD and TEM results for $(NiO)_{0.4}$ $(Ag_2O)_{0.6}$ NPs at different calcined temperatures

Calcined temperature (°C)	Particle size (nm)	Crystallite size (nm)
500	26.0	25.4
600	29.5	29.9
700	35.5	34.2
800	38.5	37.0

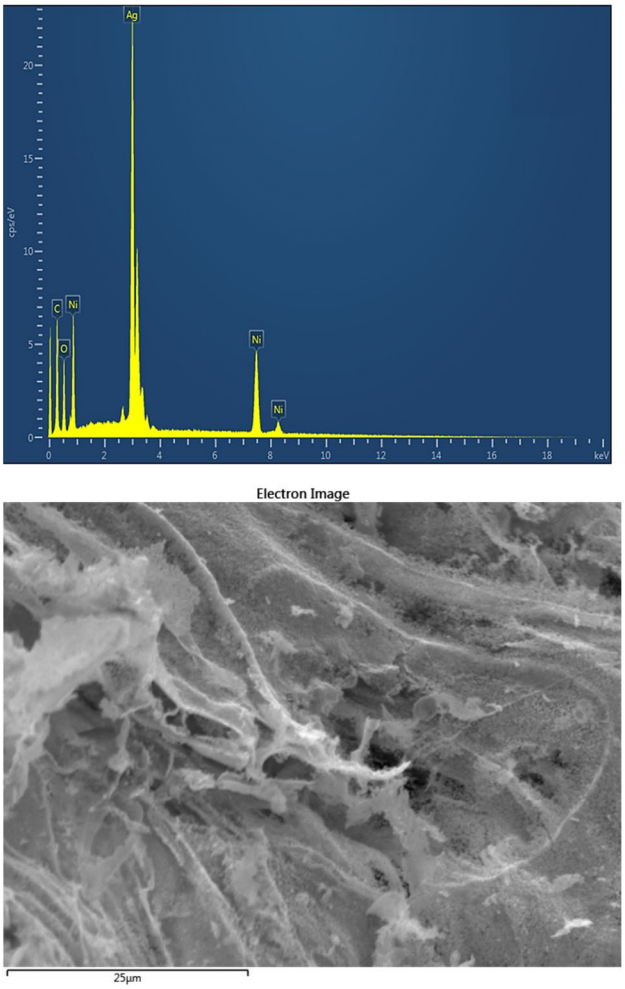

Fig. 4 EDX spectra of the $(NiO)_{0.4}$ $(Ag_2O)_{0.6}$ NPs calcined at 700 °C

XPS technique determined the chemical state, purity, and composition of the prepared NPs. The XPS pattern of $(NiO)_{0.4}$ $(Ag_2O)_{0.6}$ NPs calcined at 700 °C is shown in Fig. 5. The XPS spectra show two main peaks of 3d at 374.3 and 368.3 eV binding energies, which corresponded to Ag particles. Also, four peaks were found for 2p at 880.9, 872.9, 862.0, and 855.5 eV, which were assigned for Ni. One main peak was found for 1 s O at an energy of 529.4 eV. The binding energies of Ag $3d_{5/2}$ at 368.3 eV [51, 52] and Ag $3d_{3/2}$ at 374.3 eV were corresponded to Ag_2O [52]. Binding energies of 855.5 and 872.9 were related to Ni $2p_{3/2}$ and Ni $2p_{1/2}$, respectively, for 2 + oxidation state [53]. Also, binding energies of 862.0 eV and 880.9 eV were correlated with Ni $2p_{3/2}$ (satellite) and Ni $2p_{1/2}$ (satellite) [51]. In oxygen, the binding energy of 529.4 eV confirms the existence of two oxygen types. This means that NiO and Ag_2O have pure oxidation states [53].

3.4 Morphological characterization

Four samples were investigated and analyzed by TEM after thermal treatment and removal of PVP at four different calcined temperatures. As found earlier by XRD, crystallinity was enhanced as the temperature increased, and hence, NPs were formed as shown in Fig. 6. Homogeneous morphology is also observed from TEM images in Fig. 6a-d. Uniform spherical shape was also verified from which the particle size was calculated for each calcined sample. The particle size and particle size distribution of $(NiO)_{0.4}$ $(Ag_2O)_{0.6}$ NPs were gradually increased from 26.0 nm at 500 °C to 38.5 nm at 800 °C (Fig. 6a', d' and Table 1). In fact, the particles were enlarged due to the effect of increasing temperatures which caused a coalescence and adhesion to the particles. Also, higher temperatures caused surface melting to the particles producing NPs with larger sizes at 800 °C or generally at other higher temperatures. Based on the results, thermal treatment was successfully produced uniform binary $(NiO)_{0.4}$ $(Ag_2O)_{0.6}$ NPs. Also, it is worth mentioning that PVP has an important role in the formation of NPs through a restraining effect that controlled the particle size and prevented agglomeration.

3.5 Spectroscopic properties

UV–Vis analysis was performed to determine the optical band gap of the prepared NPs. The reflectance spectra of $(NiO)_{0.4}$ $(Ag_2O)_{0.6}$ NPs were calcined at 500, 600, 700, and 800 °C in a range of 200–850 nm. The optical band gaps were calculated using the Kubelka–Munk equation:

$$(F(R_\infty).h\nu)^2 = A(h\nu - E_g) \quad (2)$$

where $F(R_\infty)$ is the Kubelka–Munk function, $h\nu$ is the incident photon energy, A is a constant and R_∞ is the diffuse reflectance. To determine the band gap, the values of $(F(R_\infty).\ h\nu)^2$ were plotted against $(h\nu)$ as shown in Fig. 7. The optical band gap was evaluated by drawing a straight line to fit the experimental band gap curve and extrapolating that line to intercept the $(h\nu)$ axis [48, 54, 55]. The results showed the energy band gap (E_g) values were decreased as the temperature increased. Two band energies were found for each calcined sample that related to NiO and Ag_2O which

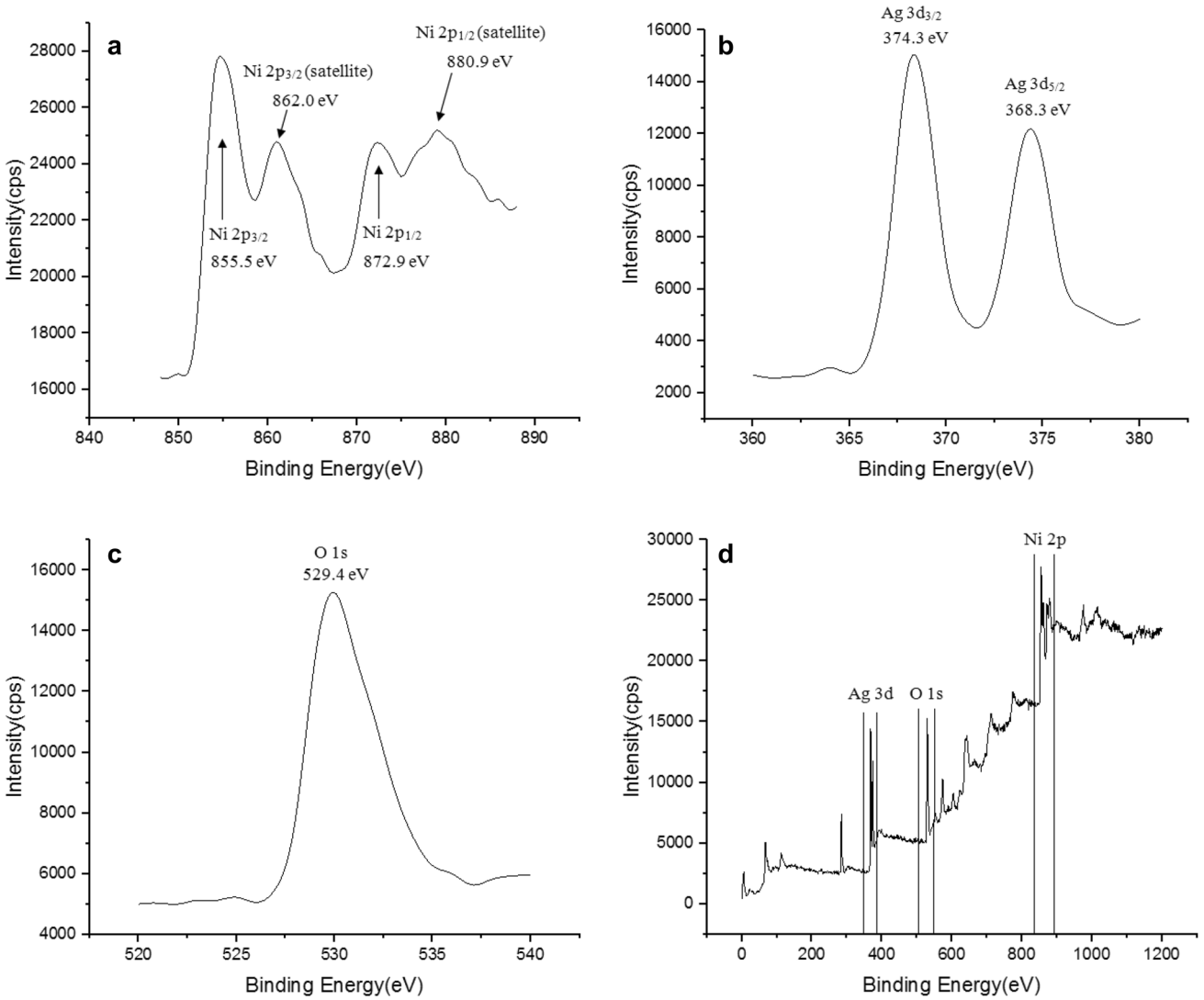

Fig. 5 XPS photoelectron spectra of the $(NiO)_{0.4}$ $(Ag_2O)_{0.6}$ NPs calcined at 700 °C for: **a** Ni 2p, **b** Ag 3d, **c** O 1 s, and **d** spectra for all regions

confirmed the production of binary $(NiO)_{0.4}$ $(Ag_2O)_{0.6}$ NPs (Table 2). The values of E_g for $(NiO)_{0.4}$ $(Ag_2O)_{0.6}$ NPs were ~ (3.05, 2.45), (2.85, 2.30), (2.75, 2.09), and (2.70, 1.95) eV at temperatures of 500, 600, 700, and 800 °C, respectively. These results were found to be compatible with findings by TEM analysis. As the temperature increased, E_g values were decreased while the particle size increased. These findings could be affected by the quantum confinement effect, which is the size quantization due to the position of electrons and holes in a confined volume of NPs [48, 53, 55].

PL analysis was conducted after excitation at 320 nm to all samples prepared at 500, 600, 700, and 800 °C, respectively. Broad emission peaks were found between ~ 423 and 771 nm. In the PL spectra (Fig. 8), two emission peaks were appeared for each temperature. This was taken as evidence for the formation of binary $(NiO)_{0.4}$ $(Ag_2O)_{0.6}$ NPs. These prominent peaks were positioned at 551–595, 551–595, 547–591, and 551–595 nm at 500, 600, 700, and 800 °C, respectively. It was found that PL intensity increased as the calcined temperature increased (Table 3). Higher temperatures enhanced the crystallinity, so the maximum PL intensity and hence the optimal crystallinity were found at 800 °C [48, 55]. In fact, the reason for the emission of visible light in oxide NPs was due to the presence of free carriers that were originated from oxygen vacancies and intrinsic defects [56]. Also, the two peaks were produced due to movement that happened between the recombination of electron–hole pairs, oxygen vacancies, and metal ions [48]. The transition for the most intense peak in each sample emitted photons with green light, whereas the less intense peak emitted photons of orange light (Table 3). Generally, PL spectra can be used as a significant tool to determine the effectiveness of charge carrier trapping and movement. The intensity which results from the recombination of electron–hole pairs is an

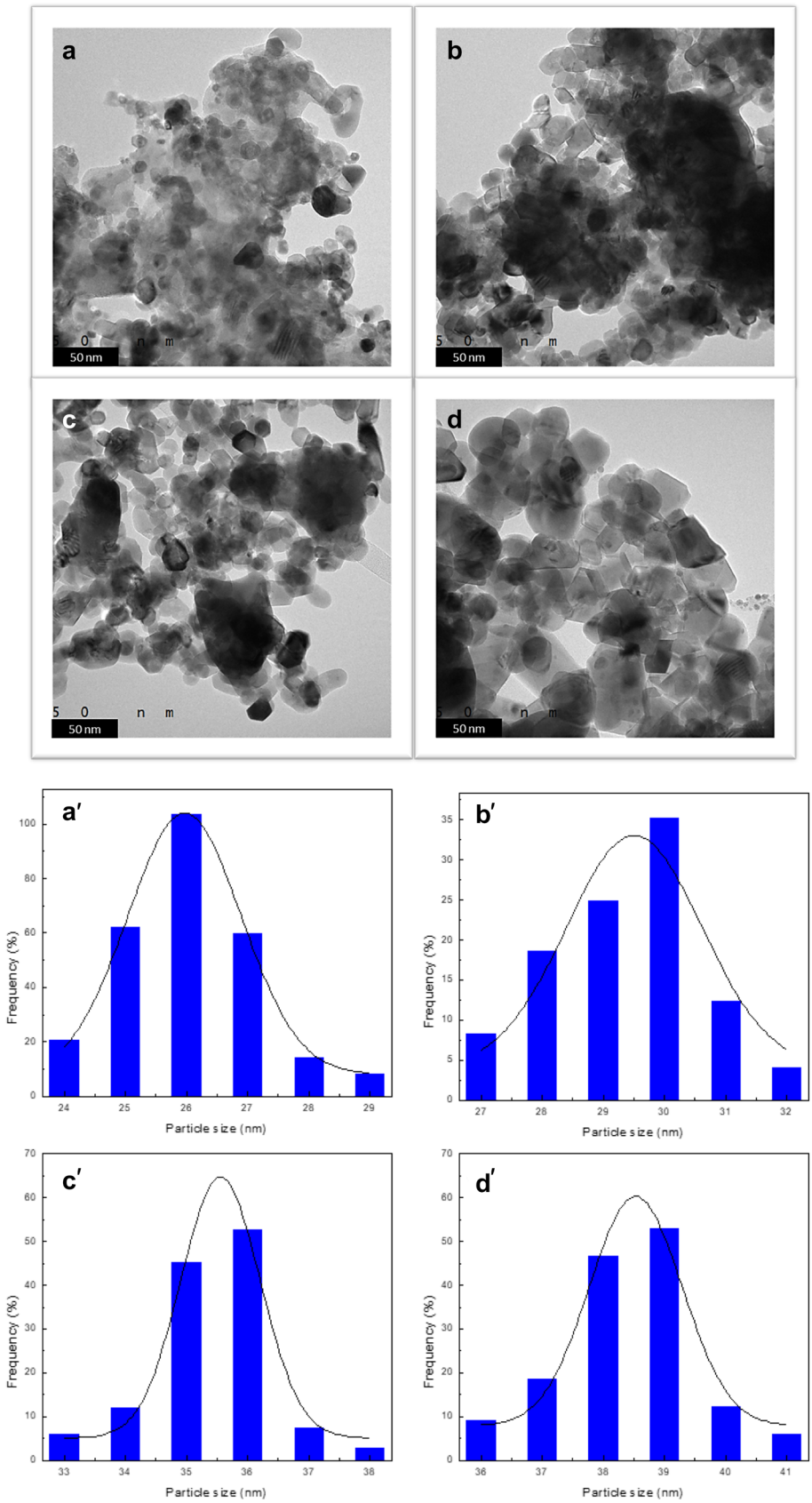

Fig. 6 TEM images (at scale of 50 nm) and related particle size distribution histograms for $(NiO)_{0.4}$ $(Ag_2O)_{0.6}$ NPs calcined at (a, a′) 500, (b, b′) 600, (c, c′) 700, and (d, d′) 800 °C

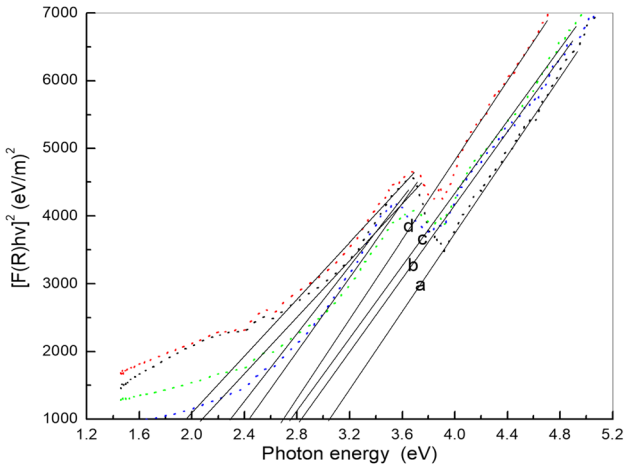

Fig. 7 Energy band gap of $(NiO)_{0.4}$ $(Ag_2O)_{0.6}$ NPs calcined at **a** 500, **b** 600, **c** 700, and **d** 800 °C

Table 2 energy band gap (eV) of $(NiO)_{0.4}$ $(Ag_2O)_{0.6}$ NPs at temperatures from 500 to 800 °C

Temp. (°C)	500	600	700	800
$(NiO)_{0.4}$	3.05	2.85	2.75	2.70
$(Ag_2O)_{0.6}$	2.45	2.30	2.09	1.95

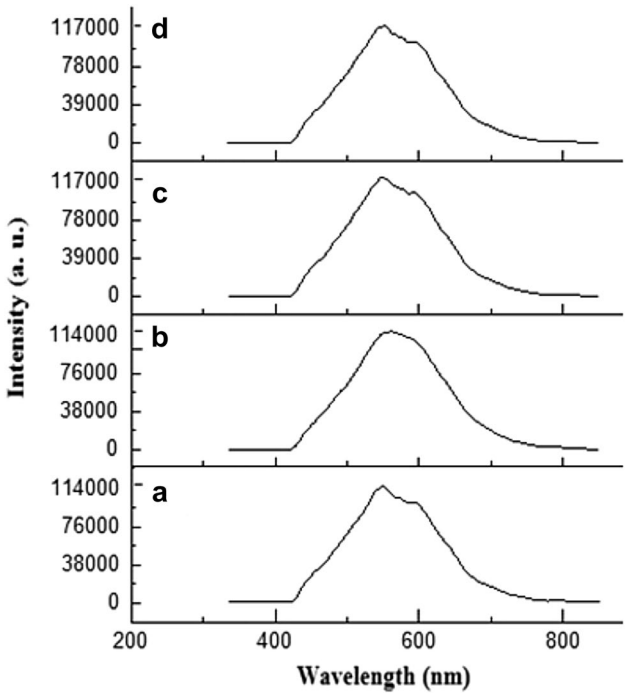

Fig. 8 PL spectra of $(NiO)_{0.4}$ $(Ag_2O)_{0.6}$ NPs synthesized at **a** 500, **b** 600, **c** 700, and **d** 800 °C

Table 3 PL data for $(NiO)_{0.4}$ $(Ag_2O)_{0.6}$ NPs prepared at different temperatures

Temp. (°C)	Wavelength (nm)	Intensity (counts/s)	Color in visible light
800	551	122,727.078	Green
	595	108,364.773	Orange
700	547	120,664.914	Green
	591	104,584.563	Orange
600	551	1,203,349.95	Green
	595	102,544.324	Orange
500	551	117,489.477	Green
	595	101,175.156	Orange

indication of the degree of photocatalytic activity for NPs [57]. In this study, the highest photocatalytic activity was found at high calcined temperature (800 °C).

4 Conclusions

In this study, the synthesis of $(NiO)_{0.4}$ $(Ag_2O)_{0.6}$ NPs was carried out by a facile thermal treatment method. The PVP behaves as a capping agent during the formation of nanoparticles that prevented the occurrence of agglomeration. XRD results showed that good crystallinity was achieved at a calcined temperature of 800 °C. The particle size was increased from 26.0 nm to 38.5 nm with increasing calcined temperature. EDX analysis confirmed the purity of the produced NPs by determining the atomic composition of silver, nickel, and oxygen. Good optical properties were found for the prepared NPs which were confirmed from PL and UV–Vis analyses. Two band gaps were observed in the prepared NPs, which allow the absorption of certain wavelengths of solar energy. So, these NPs can be used in many solar cell applications. In fact, the thermal treatment method has many advantages; simple, not expensive, no need to use many chemicals and equipment, and no toxic materials or other by-products can be produced during preparation. Also, the properties of the prepared NPs can be controlled by varying the temperature. Other parameters such as concentrations of precursors and/or PVP can be investigated in the next research. It is also highly recommended to use this eco-friendly method to prepare other metal oxides NPs, which have wide and useful applications.

References

1. M. Tadic, D. Nikolic, M. Panjan, G.R. Blake, Magnetic properties of NiO (nickel oxide) nanoparticles: Blocking temperature

and Neel temperature. J. Alloys Compd. **647**, 1061–1068 (2015). https://doi.org/10.1016/j.jallcom.2015.06.027
2. G.T. Anand, R. Nithiyavathi, R. Ramesh, S. John Sundaram, K. Kaviyarasu, Structural and optical properties of nickel oxide nanoparticles: Investigation of antimicrobial applications, Surfaces and Interfaces. 18 (2020) 100460. https://doi.org/10.1016/j.surfin.2020.100460.
3. V.E. Gurenko, V.I. Popkov, A.A. Lobinsky, Synthesis of NiO granular nanospheres as a novel material for high-performance supercapacitors. Mater. Lett. **279**, 128478 (2020). https://doi.org/10.1016/j.matlet.2020.128478
4. A.D. Khalaji, M. Jarosova, P. Machek, K. Chen, D. Xue, Facile synthesis, characterization and electrochemical performance of nickel oxide nanoparticles prepared by thermal decomposition. Scr. Mater. **181**, 53–57 (2020). https://doi.org/10.1016/j.scriptamat.2020.02.015
5. J. Singh, S. Lee, S. Kim, S.P. Singh, J. Kim, A.K. Rai, Fabrication of 1D mesoporous NiO nano-rods as high capacity and long-life anode material for lithium ion batteries. J. Alloys Compd. **850**, 156755 (2021). https://doi.org/10.1016/j.jallcom.2020.156755
6. A.M. Abdallah, H. Basma, R. Awad, Preparation, Characterization, and Application of Nickel Oxide Nanoparticles in Glucose and Lactose Biosensors. Mod. Appl. Sci. **13**, 99 (2019). https://doi.org/10.5539/mas.v13n6p99
7. K. Deevi, V.S.R. Immareddy, Synthesis and characterization of optically transparent nickel oxide nanoparticles as a hole transport material for hybrid perovskite solar cells. J. Mater. Sci. Mater. Electron. **30**, 6242–6248 (2019). https://doi.org/10.1007/s10854-019-00927-8
8. J.S. Fain, J.W. Mares, S.M. Weiss, Size-controlled nickel oxide nanoparticle synthesis using mesoporous silicon thin films, J. Nanoparticle Res. 17 (2015). https://doi.org/10.1007/s11051-015-3122-2.
9. K. Kaviyarasu, E. Manikandan, J. Kennedy, M. Jayachandran, R. Ladchumananandasiivam, U.U. De Gomes, M. Maaza, Synthesis and characterization studies of NiO nanorods for enhancing solar cell efficiency using photon upconversion materials. Ceram. Int. **42**, 8385–8394 (2016). https://doi.org/10.1016/j.ceramint.2016.02.054
10. J. Fowsiya, G. Madhumitha, Biomolecules derived from Carissa edulis for the microwave assisted synthesis of Ag2O nanoparticles: a study against S. incertulas, C. medinalis and S. mauritia, J. Clust. Sci. 30 (2019) 1243–1252. https://doi.org/10.1007/s10876-019-01627-3.
11. S. Haq, K.A. Yasin, W. Rehman, M. Waseem, M.N. Ahmed, M.I. Shahzad, N. Shahzad, A. Shah, M.U. Rehman, B. Khan, Green synthesis of silver oxide nanostructures and investigation of their synergistic effect with Moxifloxacin against selected microorganisms. J. Inorg. Organomet. Polym. Mater. (2020). https://doi.org/10.1007/s10904-020-01763-8
12. R. Li, Z. Chen, N. Ren, Y. Wang, Y. Wang, F. Yu, Biosynthesis of silver oxide nanoparticles and their photocatalytic and antimicrobial activity evaluation for wound healing applications in nursing care. J. Photochem. Photobiol. B Biol. **199**, 111593 (2019). https://doi.org/10.1016/j.jphotobiol.2019.111593
13. V. Manikandan, P. Velmurugan, J.P.W. Chang, Green synthesis of silver oxide nanoparticles and its antibacterial activity against dental pathogens. 3 Biotech. 7 (2017) 1–9. https://doi.org/10.1007/s13205-017-0670-4.
14. B.N. Rashmi, S.F. Harlapur, B. Avinash, C.R. Ravikumar, H.P. Nagaswarupa, M.R. Anil Kumar, K. Gurushantha, M.S. Santosh, Facile green synthesis of silver oxide nanoparticles and their electrochemical, photocatalytic and biological studies. Inorg. Chem. Commun. 111 (2020) 107580. https://doi.org/10.1016/j.inoche.2019.107580.
15. S.P. Vinay, G. Udayabhanu, C.P. Nagaraju, N. Chandrappa, Chandrasekhar, Novel Gomutra (cow urine) mediated synthesis of silver oxide nanoparticles and their enhanced photocatalytic, photoluminescence and antibacterial studies. J. Sci. Adv. Mater. Devices. **4**, 392–399 (2019). https://doi.org/10.1016/j.jsamd.2019.08.004
16. G. Pradheesh, S. Suresh, J. Suresh, V. Alexramani, Antimicrobial and Anticancer Activity Studies on Green Synthesized Silver Oxide Nanoparticles from the Medicinal Plant Cyathea nilgiriensis Holttum. Int. J. Pharm. Investig. **10**, 146–150 (2020). https://doi.org/10.5530/ijpi.2020.2.27
17. S. Iqbal, M. Fakhar-e-alam, F. Akbar, M. Sha, M. Atif, N. Amin, M. Ismail, A. Hanif, W.A. Farooq, Application of silver oxide nanoparticles for the treatment of cancer **1189**, 203–209 (2019). https://doi.org/10.1016/j.molstruc.2019.04.041
18. G. Maheshwaran, A. Nivedhitha Bharathi, M. Malai Selvi, M. Krishna Kumar, R. Mohan Kumar, S. Sudhahar, Green synthesis of Silver oxide nanoparticles using Zephyranthes Rosea flower extract and evaluation of biological activities. J. Environ. Chem. Eng. 8 (2020) 104137. https://doi.org/10.1016/j.jece.2020.104137.
19. T. Zahra, K.S. Ahmad, Structural, optical and electrochemical studies of organo-templated wet synthesis of cubic shaped nickel oxide nanoparticles. Optik (Stuttg). **205**, 164241 (2020). https://doi.org/10.1016/j.ijleo.2020.164241
20. A.A. Olajire, A.A. Mohammed, Green synthesis of nickel oxide nanoparticles and studies of their photocatalytic activity in degradation of polyethylene films. Adv. Powder Technol. **31**, 211–218 (2020). https://doi.org/10.1016/j.apt.2019.10.012
21. N.M. Al-Hada, H.M. Kamari, M.A. Saleh, M.H. Flaifel, A.M. Al-Ghaili, H. Kasim, A.A. Baqer, E. Saion, W. Jihua, Morphological, structural and optical behaviour of PVA capped binary (NiO)0.5 (Cr2O3)0.5 nanoparticles produced via single step based thermal technique, Results Phys. 17 (2020) 103059. https://doi.org/10.1016/j.rinp.2020.103059.
22. D. Thakur, A. Sharma, D.S. Rana, N. Thakur, D. Singh, T. Tamulevicius, M. Andrulevicius, Facile synthesis of silver-doped zinc oxide nanostructures as efficient scaffolds for detection of p-Nitrophenol. (2020).
23. K. Prikhodko, A. Nasriddinov, S. Vladimirova, M. Rumyantseva, A. Gaskov, Nanocrystalline oxides Ni x Co3− x O4 : Sub-ppm H 2 S Sensing and Humidity Effect. (2021).
24. Z. Fereshteh, M. Salavati-Niasari, K. Saberyan, S.M. Hosseinpour-Mashkani, F. Tavakoli, Synthesis of nickel oxide nanoparticles from thermal decomposition of a new precursor. J. Clust. Sci. **23**, 577–583 (2012). https://doi.org/10.1007/s10876-012-0477-8
25. M. Hashem, E. Saion, N.M. Al-Hada, H.M. Kamari, A.H. Shaari, Z.A. Talib, S.B. Paiman, M.A. Kamarudeen, Fabrication and characterization of semiconductor nickel oxide (NiO) nanoparticles manufactured using a facile thermal treatment. Results Phys. **6**, 1024–1030 (2016). https://doi.org/10.1016/j.rinp.2016.11.031
26. Z.H. Dhoondia, H. Chakraborty, Lactobacillus mediated synthesis of silver oxide nanoparticles, Nanomater. Nanotechnol. 2 (2012). https://doi.org/10.5772/55741.
27. M.R.H. Siddiqui, S.F. Adil, M.E. Assal, R. Ali, A. Al-Warthan, Synthesis and characterization of silver oxide and silver chloride nanoparticles with high thermal stability, Asian J. Chem. 25 (2013) 3405–3409. https://doi.org/10.14233/ajchem.2013.13874.
28. M.M. Rahman, S.B. Khan, A. Jamal, M. Faisal, A.M. Asiri, Highly sensitive methanol chemical sensor based on undoped silver oxide nanoparticles prepared by a solution method, (2012) 99–106. https://doi.org/10.1007/s00604-012-0817-2.
29. H. Baksh, J.A. Buledi, N.H. Khand, A.R. Solangi, A. Mallah, S.T. Sherazi, M.I. Abro, Ultra-selective determination of carbofuran by electrochemical sensor based on nickel oxide nanoparticles

stabilized by ionic liquid. Monatshefte Fur Chemie. **151**, 1689–1696 (2020). https://doi.org/10.1007/s00706-020-02704-4
30. L.M. Lyu, W.C. Wang, M.H. Huang, Synthesis of Ag2O nanocrystals with systematic shape evolution from cubic to hexapod structures and their surface properties. Chem. A Eur. J. **16**, 14167–14174 (2010). https://doi.org/10.1002/chem.201000563
31. W.M. Shume, H.C.A. Murthy, E.A. Zereffa, A review on synthesis and characterization of Ag2O nanoparticles for photocatalytic applications. J. Chem. 2020 (2020). https://doi.org/10.1155/2020/5039479.
32. S. Ahmad, H. Rashid, Q. Jalil, S. Munir, S. Khan, Barkatullah, R. Ullah, A.A. Shahat, A.A.N.A. A-Mishari, A.A. Shahat, H.M. Mahmood, A. Bari, Polymers encapsulated aspirin loaded silver oxide nanoparticles: Synthesis, characterization and its bio-applications, Sains Malaysiana. 48 (2019) 1887–1897. https://doi.org/10.17576/jsm-2019-4809-09.
33. S.M. Hosseinpour-Mashkani, M. Ramezani, Silver and silver oxide nanoparticles: synthesis and characterization by thermal decomposition. Mater. Lett. **130**, 259–262 (2014). https://doi.org/10.1016/j.matlet.2014.05.133
34. N.L. Yong, A. Ahmad, A.W. Mohammad, Synthesis and characterization of silver oxide nanoparticles by a novel method **4**, 155–158 (2013)
35. F.T. Thema, E. Manikandan, A. Gurib-Fakim, M. Maaza, Single phase Bunsenite NiO nanoparticles green synthesis by Agathosma betulina natural extract. J. Alloys Compd. **657**, 655–661 (2016). https://doi.org/10.1016/j.jallcom.2015.09.227
36. M.I. Din, A.G. Nabi, A. Rani, A. Aihetasham, M. Mukhtar, Single step green synthesis of stable nickel and nickel oxide nanoparticles from Calotropis gigantea: Catalytic and antimicrobial potentials. Environ. Nanotechnol. Monit. Manag. **9**, 29–36 (2018). https://doi.org/10.1016/j.enmm.2017.11.005
37. B. Yu, T. Ayvalı, E. Raine, T. Li, M.M.J. Li, J. Zheng, S. Wu, A.A. Bagabas, S.C.E. Tsang, Enhanced propylene oxide selectivity for gas phase direct propylene epoxidation by lattice expansion of silver atoms on nickel nanoparticles. Appl. Catal. B Environ. **243**, 304–312 (2019). https://doi.org/10.1016/j.apcatb.2018.10.061
38. M.M. Mohammadi, S.S. Gunturi, S. Shao, S. Konda, R.D. Buchner, M.T. Swihart, Flame-synthesized nickel-silver nanoparticle inks provide high conductivity without sintering. Chem. Eng. J. **372**, 648–655 (2019). https://doi.org/10.1016/j.cej.2019.04.141
39. J.J. Jing, J. Xie, G.Y. Chen, W.H. Li, M.M. Zhang, Preparation of nickel–silver core–shell nanoparticles by liquid-phase reduction for use in conductive paste. J. Exp. Nanosci. **10**, 1347–1356 (2015). https://doi.org/10.1080/17458080.2015.1012751
40. S. Senapati, S.K. Srivastava, S.B. Singh, H.N. Mishra, Magnetic Ni/Ag core-shell nanostructure from prickly Ni nanowire precursor and its catalytic and antibacterial activity. J. Mater. Chem. **22**, 6899–6906 (2012). https://doi.org/10.1039/c2jm00143h
41. Y. Thaver, S.O. Oseni, G. Tessema, Silver doped nickel oxide nanocomposite and photon harvesting enhancement in bulkheterojunction organic solar cell. Sol. Energy. **214**, 11–18 (2021). https://doi.org/10.1016/j.solener.2020.11.044
42. S. Ghazal, A. Akbari, H.A. Hosseini, Z. Sabouri, F. Forouzanfar, M. Khatami, M. Darroudi, Biosynthesis of silver-doped nickel oxide nanoparticles and evaluation of their photocatalytic and cytotoxicity properties. Appl. Phys. A Mater. Sci. Process. **126**, 1–8 (2020). https://doi.org/10.1007/s00339-020-03664-6
43. C. Liu, D. Xie, P. Liu, S. Xie, S. Wang, F. Cheng, M. Zhang, L. Wang, Voltammetric determination of levofloxacin using silver nanoparticles deposited on a thin nickel oxide porous film. Microchim. Acta. 186 (2019). https://doi.org/10.1007/s00604-018-3146-2.
44. S. Nagamuthu, K.S. Ryu, Synthesis of Ag/NiO Honeycomb structured nanoarrays as the electrode material for high performance asymmetric supercapacitor devices. Sci. Rep. **9**, 1–11 (2019). https://doi.org/10.1038/s41598-019-41446-0
45. M.Z. Iqbal, R.J. Kriek, Silver/Nickel Oxide (Ag/NiO) Nanocomposites produced via a Citrate Sol-Gel route as electrocatalyst for the oxygen evolution reaction (OER) in alkaline medium. Electrocatalysis **9**, 279–286 (2018). https://doi.org/10.1007/s12678-018-0455-5
46. W. Zhao, N. Du, H. Zhang, D. Yang, Silver-nickel oxide core-shell nanoflower arrays as high-performance anode for lithium-ion batteries. J. Power Sources. **285**, 131–136 (2015). https://doi.org/10.1016/j.jpowsour.2015.03.088
47. W. Zhao, N. Du, H. Zhang, D. Yang, Silver-nickel oxide core-shell nanoparticle array electrode with enhanced lithium-storage performance. Electrochim. Acta. **174**, 893–899 (2015). https://doi.org/10.1016/j.electacta.2015.04.156
48. N.M. Al-Hada, E. Saion, H.M. Kamari, M.H. Flaifel, A.H. Shaari, Z.A. Talib, N. Abdullahi, A.A. Baqer, A. Kharazmi, Structural, morphological and optical behaviour of PVP capped binary (ZnO)0.4 (CdO)0.6 nanoparticles synthesised by a facile thermal route. Mater. Sci. Semicond. Process. 53 (2016) 56–65. https://doi.org/10.1016/j.mssp.2016.06.004.
49. R. Bharthasaradhi, L.C. Nehru, Structural and phase transition of α- Al2O3 powders obtained by co-precipitation method. Phase Transitions **89**, 77–83 (2016). https://doi.org/10.1080/01411594.2015.1072628
50. M.A. Abd, A.H. Ali, A.N. Abd, Investigation and characterization of simple chemical method synthesized CdO-NiO nancomposite. J. Phys. Conf. Ser. 1234 (2019). https://doi.org/10.1088/1742-6596/1234/1/012051.
51. D.A. Svintsitskiy, M.K. Lazarev, T.Y. Kardash, E.A. Fedorova, E.M. Slavinskaya, A.I. Boronin, Mixed silver-nickel oxide AgNiO2: probing by CO during XPS study. J. Chem. Phys. 152 (2020). https://doi.org/10.1063/1.5138237.
52. A.Y. Vasil'kov, R.I. Dovnar, S.M. Smotryn, N.N. Iaskevich, A. V. Naumkin, Plasmon resonance of silver nanoparticles as a method of increasing their antibacterial action. Antibiotics. 7 (2018). https://doi.org/10.3390/antibiotics7030080.
53. N.M. Al-Hada, A.M. Al-Ghaili, H. Kasim, M.A. Saleh, H. Baqiah, J. Liu, J. Wang, Nanofabrication of (Cr2O3)x (NiO)1–x and the impact of precursor concentrations on nanoparticles conduct. J. Mater. Res. Technol. **11**, 252–263 (2021). https://doi.org/10.1016/j.jmrt.2021.01.007
54. N.M. Al-Hada, H.M. Kamari, M.A. Saleh, M.H. Flaifel, A.M. Al-Ghaili, H. Kasim, A.A. Baqer, E. Saion, W. Jihua, Morphological, structural and optical behaviour of PVA capped binary (NiO)0.5 (Cr2O3)0.5 nanoparticles produced via single step based thermal technique. Results Phys. 17 (2020) 103059. https://doi.org/10.1016/j.rinp.2020.103059.
55. A.A. Baqer, K.A. Matori, N.M. Al-Hada, A.H. Shaari, H.M. Kamari, E. Saion, J.L.Y. Chyi, C.A.C. Abdullah, Synthesis and characterization of binary (CuO)0.6(CeO2)0.4 nanoparticles via a simple heat treatment method. Results Phys. 9 (2018) 471–478. https://doi.org/10.1016/j.rinp.2018.02.079.
56. A. Pahlavan, H. Karimi-Maleh, F. Karimi, M.A. Amiri, Z. Khoshnama, M.R. Shahmiri, M. Keyvanfard, Application of CdO nanoparticle ionic liquid modified carbon paste electrode as a high sensitive biosensor for square wave voltammetric determination of NADH. Mater. Sci. Eng. C. **45**, 210–215 (2014). https://doi.org/10.1016/j.msec.2014.09.013
57. S. Muhamad, H. Mohamed Kamari, N.M. Al-Hada, C.A.C. Abdullah, N.N.S. Nidzam, Fabrication of binary (ZnO)x(TiO2)1−x nanoparticles via thermal treatment route and evaluating the impact of various molar concentrations on the structure and optical behaviors. Appl. Phys. A Mater. Sci. Process. 126 (2020) 1–15. https://doi.org/10.1007/s00339-020-03701-4.